CONTINUUM MODELING OF ENGINEERING CONSTANTS OF ORIENTED STRANDBOARD

Jong N. Lee†
Postdoctoral Researcher

and

Qinglin Wu†
Associate Professor
School of Renewable Natural Resources
Louisiana State University Agricultural Center
Baton Rouge, LA 70803-6202

(Received January 2002)

ABSTRACT

A two-dimensional model to predict engineering constants of oriented strandboard (OSB) was developed using a continuum theory. The orthotropic flake properties, flake alignment distribution, and panel shelling ratio (as measured by flake weight ratio, FWR, between face layer and entire board) for three-layer OSB were considered in the model.

The two-term cosine probability density function (PDF) provided an effective way to describe flake alignment distributions for both single and three-layer OSB based on flake angle measurements from the panel top surface. The parameters that define the PDF varied with percent alignment (PA) and FWR. The continuum model, combined with flake alignment PDFs, predicted general trends of changes in OSB's engineering constants including Young's moduli, shear modulus, Poisson ratio, and linear expansion (LE) coefficients. The predicted values Young's moduli and LE along the two major directions compared well with experimental data for selected board structures. The three-dimensional mesh plots on various properties allow examining the trend of change of each property as a function of PA and FWR, which can be used to optimize OSB's engineering performance.

The continuum model provides a comprehensive analytical solution for the prediction of two-dimensional engineering constants of OSB, which is the basis for future modeling on OSB's void structure.

Keywords: Flake alignment distribution, in-plane modulus, laminate modeling, linear expansion coefficient, structural panel.

INTRODUCTION

Considerable amount of work has been done to correlate mechanical and swelling properties of structural oriented strandboard (OSB) to various processing variables including board density, resin content, and flake alignment level (Kelly 1977; Geimer 1979; Wu 1999). Establishment of quantitative relationships among the variables is typically limited to empirical modeling of experimental data collected from extensive laboratory testing. This is probably due to the fact that the orthotropy of the constituent oriented strand matrix considerably increases the complexity of the mechanical analysis. Attempts have been made to develop theoretical models for the prediction of elastic constants and linear expansion (LE) of OSB (Hunt and Suddarth 1974; Shaler and Blankenhorn 1990; Xu and Suchsland 1997; Xu 2000; Barnes 2000; Lee and Wu 2002). However, flakes as orthotropic planar components, flake alignment distribution (FAD), thermal/mechanical modification of flake properties, panel shelling ratio (as measured by flake weight ratio, FWR, – weight proportion of flakes in the face layer

† Member of SWST.

Wood and Fiber Science, 35(1), 2003, pp. 24–40
© 2003 by the Society of Wood Science and Technology

to the total flake weight) for three-layer boards have not been fully addressed. Thus, the need for more comprehensive models with simulation capability of individual and interaction effects of various processing parameters on panel's engineering constants is clearly needed.

As a primary constituent material in OSB, wood flakes have their intrinsic mechanical and dimensional properties, which are influenced by resin application and heat treatments. These factors need be considered in the modeling of OSB's engineering constants. Price (1976) and Geimer et al. (1985) measured tensile properties of individual flakes cut from sweetgum and Douglas-fir logs before and after hot-pressing. It was shown that tensile properties of the flakes varied with the positions at which they were placed in the mat (i.e., face or core layers) due to different degrees of thermal and mechanical modification during hot-pressing. Tensile modulus for flakes placed in the face layer increased by hot-pressing, while those in the core layer showed a decrease. However, information on the flake-adhesive system as affected by thermo-mechanical modification of flakes during hot-pressing has not been provided. To take into account the adhesive effect, the Halpin and Tsai equation (1967) was used by Shaler and Blankenhorn (1990) in predicting properties of the flake-adhesive system.

Both mechanical and physical properties of OSB are highly related to FAD (Geimer 1976; Steinmetz and Polley 1974). Geimer (1976) proposed to measure the extent of flake alignment using percent alignment (PA). Harris and Johnson (1982) emphasized the use of a statistical distribution to describe the alignment level. They preferred the von Mises distribution to normal distribution and showed that the extent of alignment in flake-type composites can be described by a mean flake angle and a concentration parameter. Several other studies were conducted to predict elastic properties of paper and fibrous composites in terms of FAD of various forms. These include a single-parameter exponential function (Chin et al. 1988), a truncated Fourier series with two-term cosine function (Lu et al. 1995), and a wrapped Cauchy model (Schulgasser 1985) of the von Mises distribution.

Two approaches (i.e., network and laminate) are available in predicting elastic constants of fibrous products. Network theories have been successfully used to predict in-plane density variation of flake-type composites (Dai and Steiner 1994a, b). When used to predict mechanical properties of a wood composite product, however, the theories fall short if flakes in the product are too closely packed to act as elements of a network. Furthermore, the theories require many geometrical and material parameters that are difficult to determine experimentally. Laminate (or composite) theories consider a well-bond panel as a layered plate rather than as a fiber network (Tsai and Hahn 1980; Salmen and Rigdahl 1985). OSB may then be viewed as a composite material with flake-adhesive layers as the main building unit. Laminate theories are widely used to predict the elastic moduli (Tsai and Hahn 1980; Chin et al. 1988) and hygroexpansion coefficients (Lu et al. 1995) of fibrous composites and paper. Chin et al. (1988) developed a laminate model for elastic modulus of short fiber-reinforced thermoplastics. Its application to OSB has not been attested.

This study forms part of a larger investigation on the effect of voids on engineering constants of OSB. In this work, a continuum model combining several mathematical theories was developed for solid OSB panels. The specific objectives of this study were:

1. To predict orthotropic engineering constants of the solid OSB as influenced by FAD and FWR using a continuum approach; and
2. To validate the model prediction by comparing predicted values with published experimental data by Wu (1999) and Lee and Wu (2002) for OSB with various constructions.

CONTINUUM MODELING

Flake alignment distribution (FAD)

The alignment angle of an individual flake in an OSB is defined in Fig. 1 in relation to

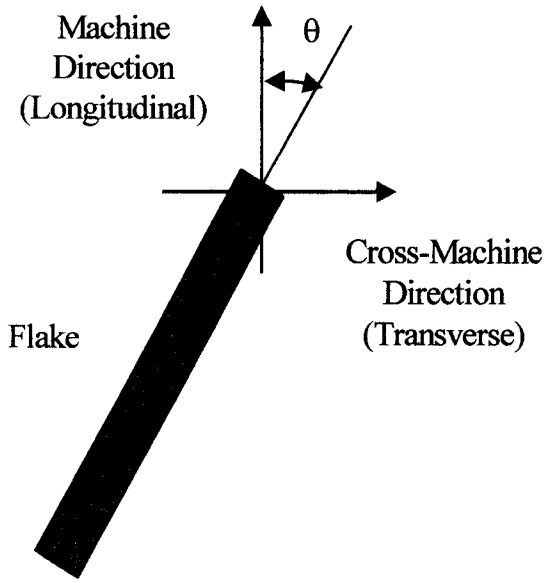

FIG. 1. Flake orientation in relation to the machine (longitudinal) and cross-machine (tranverse) directions for a given board.

the machine direction (MD) and cross-machine direction (CD) of the panel. It is assumed that the alignment distribution is governed by the von Mises probability distribution (Harris and Johnson 1982). A truncated Fourier transformation of the distribution, expressed by a two-term cosine probability density function (PDF), has the following form:

$$\pi f(\theta) = 1 + a_1 \cos 2\theta + a_2 \cos 4\theta \quad (1)$$

where, $f(\theta)$ is a probability density of the flake alignment distribution, a_1 and a_2 are the shape parameters which can be determined by fitting the experimental data on flake alignment distributions. Only cosines need be included in Eq. (1) since the distribution should be symmetric with respect to the MD and of these only even cosines need be included since the distribution would be symmetric with respect to the CD. Using this simplified PDF, extensional stiffness required in the laminate theory can be derived.

Effective moduli of the flake-adhesive system

The main components of OSB are wood flakes and adhesive. In this system, the adhesive is considered as matrix and flakes are as fibers. It is assumed that a single-ply flake-adhesive system represents the fundamental structural element of the continuum model in this study. The effective engineering constants of the unidirectional flake-adhesive system can then be predicted according to the micro-mechanics equations by Halpin and Tsai (1969):

$$M_c/M_m = (1 + \eta\zeta V_f)/(1 - \eta V_f) \quad \text{with}$$

$$\eta = (M_f/M_m - 1)/(M_f/M_m + \zeta) \quad (2)$$

where

$$\xi_{E_1} = 2(l/d); \qquad \zeta_{E_2} = 2; \quad \text{and} \quad \zeta_{G_{12}} = 1$$

where M_f, M_m, and M_c are elastic moduli of flake, adhesive, and composite system, d and l are flake thickness and length, V_f is volume fraction of fiber (flake), 1 and 2 are the principal directions of a wood flake (Fig. 2), and ζ_{E_1}, ζ_{E_2}, and $\zeta_{G_{12}}$ are the model parameters for the calculation of composite properties E_1, E_2, and G_{12}, respectively. In Eq. (2), flake discontinuity and geometry in predicting effective composite properties are considered. The model was chosen in the light of the work by Shaler and Blankenhorn (1990) for its reasonably predictive accuracy of flakeboard properties.

Laminate model

It is assumed that the principal structure unit of OSB is resin-coated wood flakes and the panel is constructed as a set of imaginary flake-adhesive layers stacked up according to the flake orientation distribution (Fig. 2). Based on the laminate plate theory (Jones 1975), it can be shown that the constitutive relation for such a panel is:

$$\begin{bmatrix} N_L \\ N_T \\ N_{LT} \end{bmatrix} + \begin{bmatrix} F_L \\ F_T \\ F_{LT} \end{bmatrix} = \begin{bmatrix} A_{11} & A_{12} & A_{16} \\ A_{12} & A_{22} & A_{26} \\ A_{16} & A_{26} & A_{66} \end{bmatrix} \left(\begin{bmatrix} \varepsilon_L \\ \varepsilon_T \\ \gamma_{LT} \end{bmatrix} + \begin{bmatrix} e_L \\ e_T \\ e_{LT} \end{bmatrix} \right) \quad (3)$$

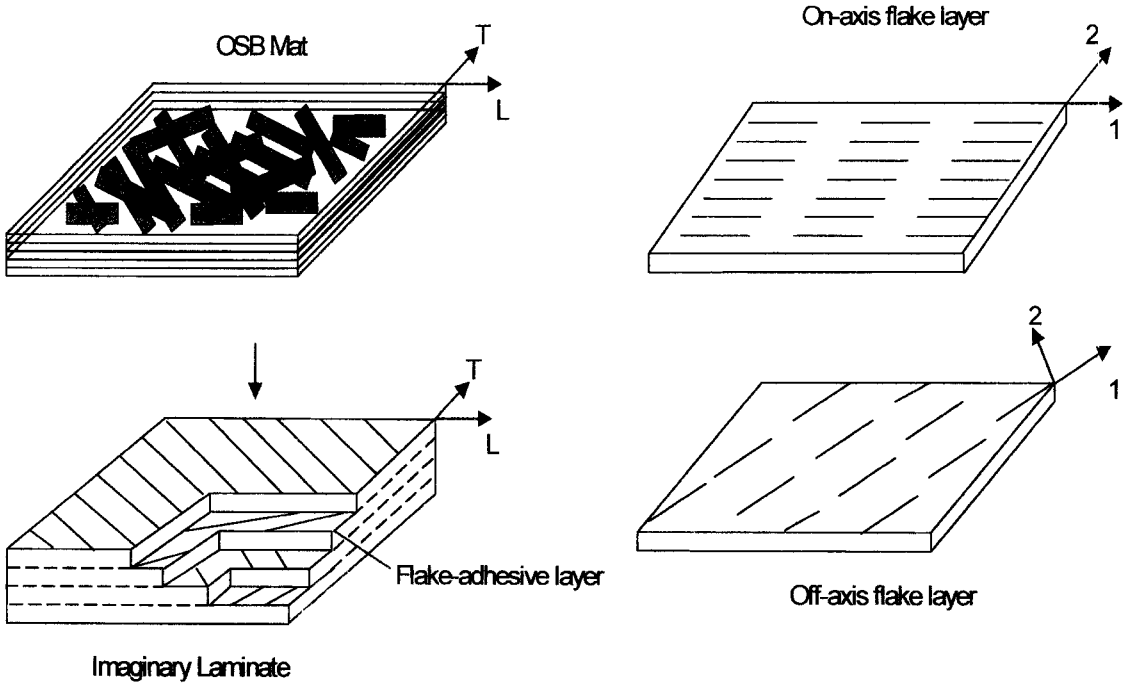

FIG. 2. A schematic of the simulated laminate model for OSB. OSB mat: showing two principal directions (L and T) of the board; Imaginary laminate: showing flake layer orientation in relation to the principal directions of the board; On-axis flake layer: showing a flake layer aligned in the principal directions of the board; and Off-axis flake layer: showing a flake layer not aligned in the principal directions of the board.

where [N_L, N_T, and N_{LT}] are the mechanical stress resultants, [F_L, F_T, and F_{LT}] are the hygroscopic swelling and shrinking forces, A_{ij} is the extensional stiffness of the laminate (i, j = 1, 2, 6), [ε_L, ε_T, and γ_{LT}] are the mechanical strains, [e_L, e_T, and e_{LT}] are the moisture-induced strains, and L and T denote panel principal directions (Fig. 2).

For a continuous distribution of flake orientation, the extensional stiffness A_{ij} can be written in the following form:

$$A_{ij} = h \int_{-\pi/2}^{\pi/2} \bar{Q}_{ij}(\theta) f(\theta)\, d\theta \quad \text{for i, j = 1, 2, 6} \tag{4}$$

where $\bar{Q}_{ij}$ is the off-axis reduced-ply stiffness, θ is the rotation angle, and h is the layer thickness. $\bar{Q}_{ij}$ in the above equations can be obtained by the following relationships (Jones 1975):

$$\begin{aligned}
\bar{Q}_{11} &= U_1 + U_2\cos 2\theta + U_3\cos 4\theta;\\
\bar{Q}_{22} &= U_1 - U_2\cos 2\theta + U_3\cos 4\theta;\\
\bar{Q}_{12} &= U_4 - U_3\cos 4\theta;\\
\bar{Q}_{16} &= -U_2/2 \sin 2\theta - U_3\sin 4\theta;\\
\bar{Q}_{26} &= -U_2/2 \sin 2\theta + U_3\sin 4\theta;\\
\bar{Q}_{66} &= U_5 - U_3\cos 4\theta
\end{aligned} \tag{5}$$

where U_i (i = 1, 2, 3, 4, and 5) are rotation stiffness invariants. They are defined as:

$$\begin{aligned}
U_1 &= (3Q_{11} + 3Q_{22} + 2Q_{12} + 4Q_{66})/8;\\
U_2 &= (Q_{11} - Q_{22})/2;\\
U_3 &= (Q_{11} + Q_{22} - 2Q_{12} - 4Q_{66})/8;\\
U_4 &= (Q_{11} + Q_{22} + 6Q_{12} - 4Q_{66})/8;\\
U_5 &= (Q_{11} + Q_{22} - 2Q_{12} + 4Q_{66})/8
\end{aligned} \tag{6}$$

with

$$Q_{11} = E_1/(1 - \nu_{12}\nu_{21});$$

$$Q_{12} = \nu_{12}E_2/(1 - \nu_{12}\nu_{21});$$

$$Q_{22} = E_2/(1 - \nu_{12}\nu_{21}); \qquad Q_{66} = G_{12} \quad (7)$$

In Eq. (7), E_1 and E_2 are the Young's moduli along the principal directions, G_{12} is the shear modulus, ν_{12} and ν_{21} are the Poisson ratios of the flake-adhesive layer, 1 and 2 are the principal directions of flakes. After substituting $\bar{Q}_{ij}$ (Eq. 5) and $f(\theta)$ (Eq. 1) into Eq. (4) and integrating, one gets

$$A_{11} = h(2U_1 + a_1U_2 + a_2U_3)/2;$$

$$A_{12} = h(2U_4 - a_2U_3)/2;$$

$$A_{22} = h(2U_1 - a_1U_2 + a_2U_3)/2;$$

$$A_{66} = h(2U_5 - a_2U_3)/2;$$

$$A_{16} = 0; \qquad A_{26} = 0 \quad (8)$$

where h is the total thickness of the laminate. The expressions for Young's moduli, shear modulus, and Poisson ratio of the laminate are:

$$E_L = N_L/(h\varepsilon_L) = [A_{11} - (A_{12}^2/A_{22})]/h$$

$$E_T = N_T/(h\varepsilon_T) = [A_{22} - (A_{12}^2/A_{11})]/h$$

$$G_{LT} = N_{LT}/(h\gamma_{LT}) = A_{66}/h$$

$$\nu_{LT} = -\varepsilon_T/\varepsilon_L = A_{12}/A_{22} \quad (9)$$

The moisture-induced stress resultants, $[F_L, F_T, \text{and } F_{LT}]$, are given by:

$$\begin{Bmatrix} F_L \\ F_T \\ F_{LT} \end{Bmatrix} = \Delta M \int_{-\pi/2}^{\pi/2} \begin{bmatrix} \bar{Q}_{11} & \bar{Q}_{12} & \bar{Q}_{16} \\ \bar{Q}_{21} & \bar{Q}_{22} & \bar{Q}_{26} \\ \bar{Q}_{16} & \bar{Q}_{26} & \bar{Q}_{66} \end{bmatrix} \begin{Bmatrix} \beta_L \\ \beta_T \\ \beta_{LT} \end{Bmatrix} f(\theta) h_0 \, d\theta \quad (10)$$

where ΔM is the incremental moisture content (MC), h_0 is the initial layer thickness, and $[\beta_L, \beta_T, \text{and } \beta_{LT}]$ are the layer linear expansion coefficients that relate to the LE coefficients of the flake-resin system, β_1 and β_2, through the following relationship:

$$\begin{Bmatrix} \beta_L \\ \beta_T \\ \beta_{LT} \end{Bmatrix} = \begin{Bmatrix} \beta_1\cos^2\theta + \beta_2\sin^2\theta \\ \beta_1\sin^2\theta + \beta_2\cos^2\theta \\ 2(\beta_1 - \beta_2)\cos\theta \sin\theta \end{Bmatrix} \quad (11)$$

After substituting the two-term cosine function (Eq. 1) and integrating, one gets

$$F_L = \Delta M\left[\frac{(\beta_1 + \beta_2)}{2}(A_{11} + A_{12}) - \frac{(\beta_1 - \beta_2)}{4}[a_1(U_1 + 2U_3 - U_4) + U_2(1 + a_2)]\right] \quad (12)$$

and

$$F_T = \Delta M\left[\frac{(\beta_1 + \beta_2)}{2}(A_{12} + A_{22}) - \frac{(\beta_1 - \beta_2)}{4}[a_1(U_1 - U_4) - U_2(1 + a_2)]\right] \quad (13)$$

F_{LT} becomes zero since there exist only stresses resulting from moisture change in the L and T directions. The in-plane LE is calculated using the constitutive relationship (Eq. 3) with no external (or mechanical) forces applied. The moisture-induced strains of the laminate are obtained as:

$$e_L = [A_{22}F_L - A_{12}F_T]/(A_{11}A_{22} - A_{12}^2)$$

$$e_T = [A_{11}F_T - A_{12}F_L]/(A_{11}A_{22} - A_{12}^2) \quad (14)$$

with $e_{LT} = 0$. Finally, panel LE coefficients, β_{PL} and β_{PT}, are determined by dividing moisture-induced strains with a given MC change. The above model was used to perform simulation analyses on OSB's engineering constants. The predicted Young's moduli and LE were compared with experimental data reported by Wu (1999) and Lee and Wu (2002) for model verification.

TABLE 1. *Engineering constants of wood flake, resin, and flake-resin system used in the model.*

Material type	Volume fraction[a] (%)	Elastic moduli				Swelling coefficient	
		E_1 (GPa)	E_2 (GPa)	G_{12} (GPa)	Poisson ratio ν_{12}/ν_{21}	β_1 (cm/cm/%)	β_2 (cm/cm/%)
Flake (F)[b]	96.6	12.71	0.896	0.960	0.37/0.0247	3.3×10^{-5}	1.5×10^{-3}
Resin (R)	3.4	7.597	7.597	0.2099	0.30/0.30	0	0
FR-system	100	12.55	0.997	0.934	0.368/0.0278	3.3×10^{-5}	1.5×10^{-3}

[a] Volume fraction of flakes and adhesive are based on 3.4% RC.
[b] Flake dimensions are 76.2 mm long, 12.7 mm wide, and 0.64 mm thick.

DERIVING MATERIAL CONSTANTS

Engineering constants of flake-adhesive system

Young's moduli, shear modulus, and Poisson ratio of southern pine solid wood were chosen and adjusted by a correction factor (Bodig and Jayne 1982; Barnes 2000) for wood flake properties (Table 1). This was done to account for flake damages and thermal modification during hot-pressing. The elastic moduli of phenol-formaldehyde resin developed by Agarwal and Broutman (1990), Hunt and Suddarth (1974), and Scala (1973) were adapted and used for the resin properties in this study (Table 1). The effective moduli for the flake-adhesive system were then calculated using Eq. (2) based on wood and resin properties, and estimated volume fractions of wood and adhesive used in the manufacture of OSB.

Because of the lack of information on linear expansion of wood flakes and resin, published LE values of solid wood in the longitudinal and transverse directions (USDA Forest Service 1987) were selected and used for the flake-resin system in the model (Table 1). The total longitudinal LE was taken as 0.1% and the transverse expansion was 4.5%, based on a 30% MC change. The relationship between LE and MC change was assumed to be linear over the entire MC range, from which the LE coefficients were calculated.

Flake alignment distribution

Flake alignment data (Wu 1999; Lee and Wu 2002) measured from the top panel surface of single- and three-layer OSB were fitted to the two-term cosine PDF (Eq. 1) to determine the parameters a_1 and a_2. The fitting was done by first calculating probabilities at various alignment angles for a given distribution. The data were then converted to cumulative probability distributions. The cumulative probability data were finally fitted to

$$\int_{-\pi/2}^{i} \left\{ \frac{1}{\pi} [1 + a_1 \cos 2\theta + a_2 \cos 4\theta] \right\} d\theta = P_i(\text{probability}) \quad (15)$$

through a technique developed by Perkins et al. (Schulgasser 1985) to determine a_1 and a_2 as the maximum likelihood estimates. In Eq. (15), p_i is the estimated cumulative probability at a specific alignment angle interval from $-\pi/2$ to i with $-\pi/2 \leq i \leq \pi/2$.

For single-layer boards, the FAD from the panel surface was assumed to run through the entire panel thickness. For three-layer boards, FADs vary with FWR at each given PA. Accordingly, the distribution from the panel surface was assumed to run through the face layer only. The distribution was turned 90 degrees for the core layer to account for the flake direction change. This could be done by selecting a desired number of face flakes (actual number depending on FWR), adding 90 degrees to their alignment angles, and treating them as core flakes in the distribution. In this work, it was done by first constructing pure face (FWR = 1) and pure core (FWR = 0) layer probability distributions. At a given FWR ($0 < \text{FWR} < 1$ for a three-layer board) and PA, the face and core probability distributions were obtained by multiplying the corresponding FWR and (1 − FWR), respectively. The entire three-layer board probability

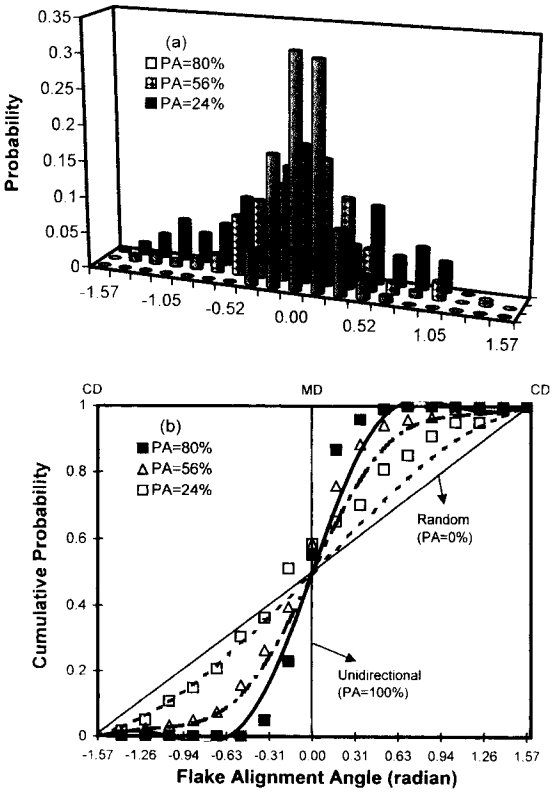

FIG. 3. Flake alignment probability density distribution of single-layer oriented strandboard from Wu (1999). (a) probability and (b) cumulative probability. Lines show values predicted by the PDF.

distribution was obtained by merging the face and core probabilities. From the probability distributions, the cumulative distributions were determined for the board. Finally, the values of parameters a_1 and a_2 in Eq. (1) were determined from Eq. (15). A nonlinear regression analysis was done to relate a_1 and a_2 with PA and FWR.

RESULTS AND DISCUSSION

Effective engineering constants of flake-adhesive system

The predicted effective moduli of the flake-adhesive system decreased in the longitudinal direction and increased in the transverse direction compared with the corresponding flake moduli (Table 1). The transverse modulus of the flake was thus reinforced by resin application. On the other hand, the longitudinal modulus of the flake was adjusted downward for the system modulus though the adjustment was small. Shear modulus of the flake-adhesive system showed a decrease compared with the wood flake modulus. In general, the degree of orthotropy of wood flakes was weakened by resin application due to the resin's isotropic properties. The Poisson ratio was affected little by resin application. LE coefficients for the system assumed the values of wood flakes.

TABLE 2. *Model parameters of the probability density function measured from panel surface of single- and three-layer boards.*

Board type	Alignment level	Percentage alignment (%)	Parameters	
			a_1	a_2
1-layer	High	82.1	1.70	1.10
	Low	61.6	1.35	0.60
	Random	24.3	−0.01	−0.15
3-layer	High	78.0	1.60	1.01
	Low	49.5	1.20	0.50

Flake alignment distribution

Single-layer distribution.—Measured flake alignment probability distributions of single-layer boards at the three alignment levels (Wu 1999) are shown in Fig. 3a. There were significant changes in the distributions as PA changed. For boards at PA = 80%, most flakes were aligned around the MD ($\theta = 0$), leading to high probability values in the range. As PA decreased (PA = 56% and 24%), more flakes were aligned towards the CD. As a result, the probability values for these boards in the MD decreased significantly, and the distribution became more widely spread over the entire angle range.

The corresponding cumulative probability distributions are shown in Fig. 3b with lines representing predictions by the two-term cosine PDF using a_1 and a_2 values shown in Table 2. All cumulative distributions are bounded by the diagonal line from the lower left corner to the upper right corner, representing completely random alignment, and the vertical

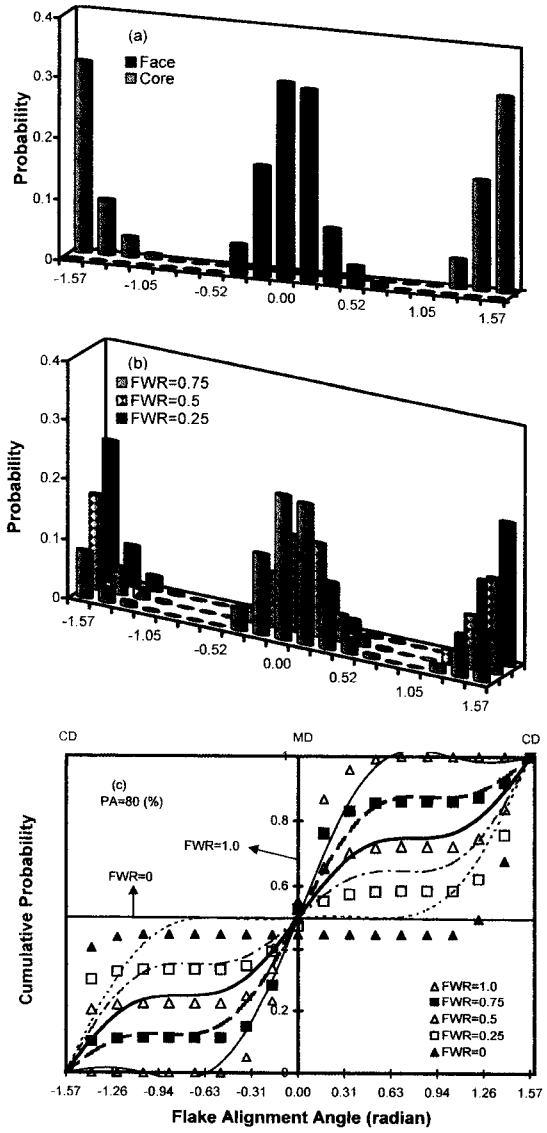

FIG. 4. Flake alignment probability density distribution of three-layer oriented strandboard. (a) pure face and core layer probabilities; (b) typical three-layer board probabilities; and (c) cumulative probability at various FWRs. Lines show values predicted by the PDF.

axis at $\theta = 0$, representing the perfect alignment. When PA = 80%, the distribution was mostly accumulated in the range of ± 0.63 radians. At PA = 56%, the probability values spread between ± 1.26 radians. At PA = 24% (randomly formed boards), the distribution became close to the diagonal line. The two-term cosine model fits the data well.

Three-layer distribution.—Pure face and core layer probability distributions at PA = 80% are shown in Fig. 4a. The face layer distribution was obtained directly from measurements on the panel surface. The core distribution was obtained by cutting the face layer distribution at $\theta = 0$ and shifting the two halves to the $\theta = \pm 1.57$ radian positions. As a result, the two distributions differed by 1.57 radians (i.e., 90 degrees), from which all three-layer board distributions were constructed. Typical three-layer board distributions are shown in Fig. 4b. As FWR decreases, i.e., the weight portion of the face flakes becomes less, the probability value decreases along the MD, and increases along the CD. The influence of FWR on the cumulative probability distribution for three-layer boards is shown in Fig. 4c with lines representing predicted values from the two-term cosine PDF. At a given PA (e.g., 80% as shown), the cumulative probability turned clockwise as FWR decreased from 1 to 0, indicating a gradual shift in the amount of flakes aligned from the MD to the CD. As shown, the two-term cosine PDF with different combinations of the shape parameters can be conveniently used to describe flake alignment probability distributions of three-layer OSB of different constructions.

Distribution function parameters.—The relationship among the model parameters (a_1 and a_2), PA, and FWR from the regression analysis has the following form:

$$a_1 = -0.00363 - 0.02493 \times PA + 0.5 \times FWR + 0.04685 \times PA \times FWR - 0.5 \times FWR^2 \qquad (R^2 = 0.75)$$

$$a_2 = +0.0522 + 0.0015 \times PA + 0.6386 \times FWR - 0.00015 \times PA^2 - 0.6386 \times FWR^2 \qquad (R^2 = 0.98) \qquad (16)$$

where PA is in percent. The values of a_1 and a_2 calculated from Eq. (16) at the selected lev-

TABLE 3. *Model parameters of the probability density function at various PAs and FWRs obtained by simulation analysis.*

FWR	Percent alignment (%)									
	0	10	20	30	40	60	60	70	80	84
					Parameter a_1					
1.0	−0.003	0.215	0.434	0.654	0.873	1.092	1.311	1.531	1.772	1.837
0.7	0.101	0.180	0.258	0.337	0.416	0.495	0.573	0.652	0.730	0.762
0.4	0.116	0.054	−0.01	−0.07	−1.13	−0.19	−0.26	−0.32	−0.38	−0.40
0.0	−0.04	−0.25	−0.50	−0.75	−1.00	−1.25	−1.59	−1.74	−1.99	−2.09
					Parameter a_2					
1.0	0.052	0.082	0.142	0.232	0.352	0.502	0.682	0.892	1.132	1.236
0.7	0.186	0.216	0.276	0.366	0.486	0.636	0.816	1.026	1.266	1.371
0.4	0.205	0.235	0.295	0.385	0.505	0.655	0.835	1.045	1.285	1.389
0.0	0.052	0.082	0.142	0.232	0.352	0.502	0.682	0.892	1.132	1.236

els of PA and FWR are summarized in Table 3 for both single- and three-layer boards.

The shape parameters predicted by Eq. (16) are plotted in three-dimensional graphs in Fig. 5 in comparison with the original data fitted from measurements on the panel surface. Parameter a_1 (Fig. 5a) increased with increases of PA and FWR. Its relationship with FWR is linear, but becomes significantly curvilinear at higher PA. Parameter a_2 (Fig. 5b) increased with increases of PA, similar to a_1. It had a symmetric relationship with FWR with peak values along the FWR = 0.5 line. This symmetric characteristics of the a_2-FWR relationship directly influenced the trend of the predicted shear modulus-FWR relationship shown later in the paper.

Simulated probability density.—Flake alignment probability densities as a function of alignment angle and PA (or FWR) were simulated using Eq. (1) with a_1 and a_2 defined by Eq. (16). Typical probability density data in relation with PA and alignment angle from 0 to 1.57 radians are shown in Fig. 6a. Along Side A (PA = 0%), the probability density was equal to a constant ($1/\pi$) at all flake alignment angles, indicating a uniform flake alignment distribution. Along Side B, the density decreased from its maximum value as flake alignment angle increased. This was due to the fact that most flakes were aligned towards the MD. As PA increased, the probability density increased in the MD (Side C), and decreased in the CD (Side D). With PA > 60%, the probability densities at flake angles $\theta > 0.628$ radians were close to zero, indicating that few flakes were aligned at these directions. The slightly upward trends of the density values in the corner range defined by Sides B and C were due to the nature of the PDF (Eq. (1)). This indicates the limitation of the two-term cosine PDF, which are further discussed later in this section.

Typical variations of probability densities as a function of FWR and alignment angle are shown in Fig. 6b. The trend was anti-symmetric with respect to the line at FWR = 0.5 due to the nature of three-layer OSB with the cross-aligned flakes. Along Side A (FWR = 0), the density increased with increases in the flake alignment angle. The opposite is true along Side B (FWR = 1.0). Along Side C (θ = 0), the probability density was the lowest when FWR = 0 (core layer only), and it increased with the increase of FWR, and reached maximum at FWR = 1.0. The opposite trend is seen along Side D (θ = 1.57 radians). The prediction of such a stereoscopic change in flake alignment distributions as affected by two major variables (PA and FWR) is helpful for optimizing the process variables related to control OSB engineering properties.

Limitation.—The shape parameters a_1 and a_2 are subjected to limits to ensure that no negative probabilities are generated. As shown in Fig. 6a, the distribution narrows from Side A

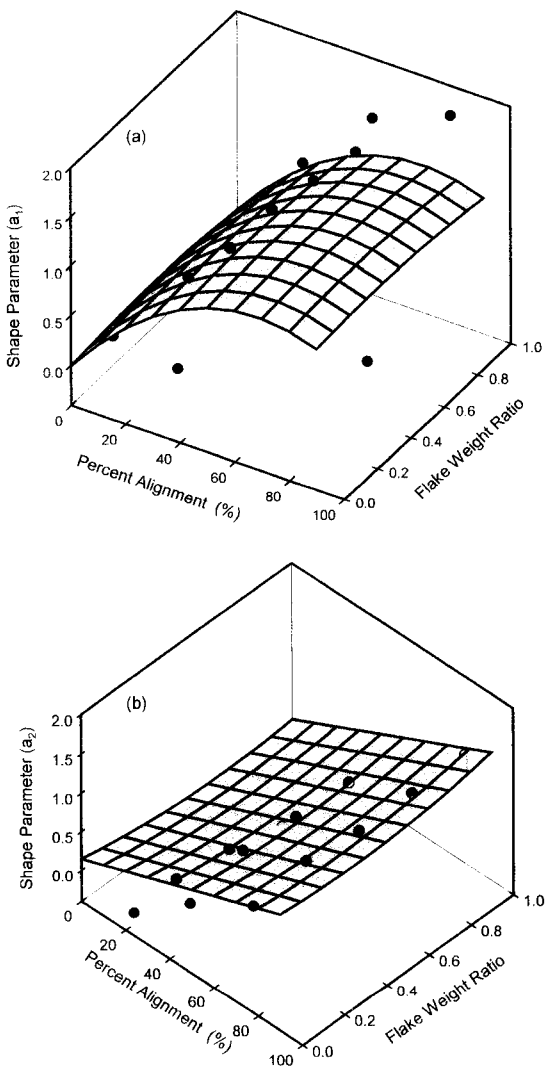

FIG. 5. Shape parameters, (a): a_1 and (b): a_2, of the flake alignment PDF. The symbols show the original data and the mesh shows the regression fits.

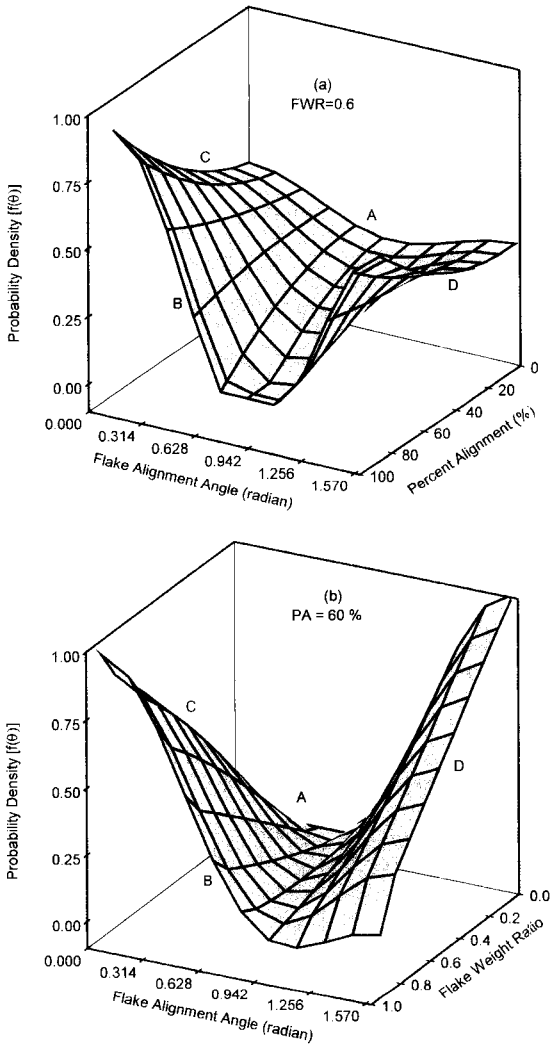

FIG. 6. Simulated probability density of flake alignment distribution as a function of flake alignment angle and PA (a) or FWR (b).

to Side B due to increasing a_2, but increases at the tail. Further increases in PA will result in negative probabilities near $\theta = \pm 1.57$ radians. It was found that Eq. (1) is only capable of providing a reliable prediction of flake alignment probability density with PA = 85% for OSB. Above the level, negative probabilities lead to erratic properties. However, due to random nature of the flake deposition process during forming, it is not practical to achieve 85% or greater alignment levels in commercial OSB. Therefore, the model, with its limitation, is considered as a useful tool for simulating OSB's engineering constants. In fact, it offers more flexibility in dealing with the combined effect of PA and FWR for three-layer OSB than any other PDF models considered. The following discussion on OSB's engineering constants is limited to PA 85% for both single- and three-layer boards.

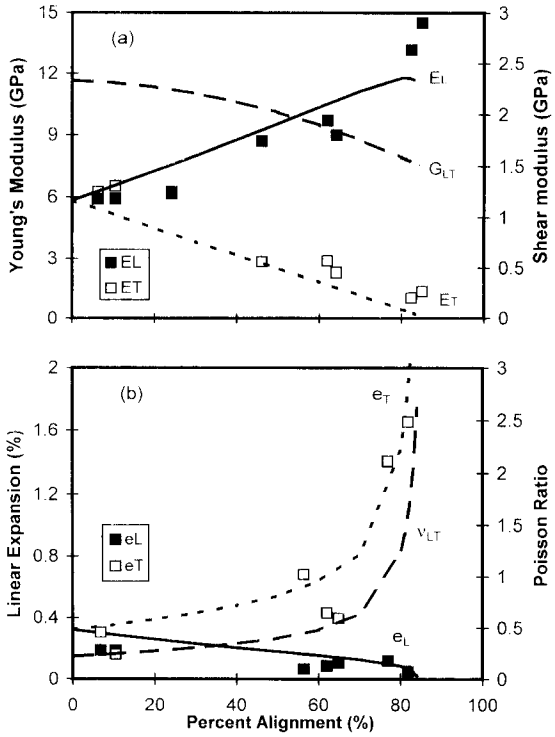

FIG. 7. Predicted elastic constants and linear expansion of single-layer OSB as a function of percent alignment. (a) E_L, E_T, and G_{LT}; (b) e_L, e_T, and ν_{LT}. Symbols show the experimental data of E_L, E_T, e_L, and e_T from boards with specific gravity = 0.7 (Wu 1999).

Engineering constants of OSB

Single-layer boards.—Predicted elastic properties of single-layer OSB as a function of PA are shown in Fig. 7a. Data at selected PAs are summarized in Table 4. For a PA change from 0 to 80%, the longitudinal modulus, E_L, increased from 5.84 to 11.78 GPa. At the same time, the transverse modulus, E_T, decreased from 5.83 to 0.45 GPa. This gave an E_L/E_T ratio of 25.92 at PA = 80%. In comparison with the experimental data from the selected boards (Wu 1999), the model predicted both longitudinal and transverse moduli reasonably well up to the 80% alignment level. The model slightly underpredicted E_L when PA increased beyond the 80% level.

Shear modulus decreased from 2.33 to 1.59 GPa with PA increased 0 to 80%. This indicates that random boards had higher shear modulus than the aligned boards. This was due to low strength values in the transverse direction for the aligned boards, which directly influenced the shear properties of OSB. The Poisson ratio, ν_{LT}, showed a curvilinear increase when PA increased (Fig. 7b). The ratio had a value greater than 1 with PA > 80%. Under high alignment levels, single-layer OSB acts like an oriented composite lumber. As found by Janowlak et al. (2001), composite lumber can have a Poisson ratio larger than 1. The upper limit of the Poisson ratio at PA =

TABLE 4. *Effective engineering constants of OSB predicted by the continuum model.*

Percent alignment (%)	Engineering constants of OSB					
	E_L (GPa)	E_T (GPa)	G_{LT} (GPa)	Poisson ratio, ν_{LT}	β_{PL} (cm/cm/%MC)	β_{PT} (cm/cm/%MC)
			Single-layer Board			
0	5.839	5.827	2.330	0.219	0.000357	0.000358
20	7.258	4.496	2.268	0.272	0.000287	0.000433
40	8.769	3.161	2.123	0.344	0.000226	0.000533
60	10.361	1.816	1.891	0.479	0.000170	0.000709
80	11.776	0.454	1.586	1.237	0.000094	0.001633
			Three-layer Board (FWR = 0.6)			
0	5.940	5.850	2.222	0.215	0.0003172	0.000360
20	6.340	5.432	2.161	0.212	0.0002981	0.000360
40	6.840	5.180	2.022	0.193	0.0002661	0.000341
60	7.350	5.045	1.791	0.156	0.0002210	0.000267
80	8.140	4.891	1.483	0.100	0.0001674	0.000227

80% for OSB was $[E_L/E_T]^{1/2} = [25.92]^{1/2} = 5.1$, based on the elasticity theory for orthotropic materials (Jones 1975). The Poisson ratio had a similar trend as the transverse LE, e_T, as shown in the graph. The predicted trends of elastic properties as influenced by PA were closely related to the values of a_1 and a_2 in the PDF of the flake alignment distribution, and their functional forms with PA. In particular, the shape of the E_L-PA curve was determined mainly by the parameter a_1, while actual modulus values were controlled by a_2.

The linear expansions along both directions for single-layer boards are shown in Fig. 7b as a function of PA. The LE coefficients (LE value divided by a 9% MC change) are summarized in Table 4. The longitudinal LE followed a linear decreasing trend as the alignment level increased up to the 85% level. Along the transverse direction, LE is expected to increase slowly with PA up to the 40% level, and the rate of increase accelerates significantly above the 60% alignment level (Wu and Suchsland 1996; Xu and Suchsland 1997; Wu 1999). The current model with the two-term cosine PDF predicts this trend closely. In fact, the PDF is one of the few analytical models which are capable of predicting the peculiar trend of e_T as influenced by PA. The predicted LEs along both directions matched the experimental data well at the selected PAs (Wu 1999). It is found that the coefficients defining the functional relationships for a_1 and a_2 influenced the LE value significantly. In addition, the transverse swelling coefficient of wood flakes also played a role in controlling the LE value of OSB.

Three-layer boards.—Engineering constants of three-layer boards as a function of PA predicted at a given panel FWR (i.e., 0.6) are shown in Fig. 8. As PA increased, more flakes were aligned along the MD. As a result, E_L increased and E_T decreased at the given FWR level (Fig. 8a). E_L had a 37% increase and E_T had a 16% decrease as PA increased from 0 to 80%. The predicted E_T agreed with the experimental data well. For E_L, there was a good agreement between measured and predicted values at low alignment levels (PA < 60%). At high PA levels (PA > 80%), the model underpredicted the modulus value. The discrepancy may be due to the fact that the prediction was based on uniform density profile across board thickness. The measured data were, however, based on results of bending tests for boards with a significant density gradient, which help increase the modulus value, especially at high alignment levels.

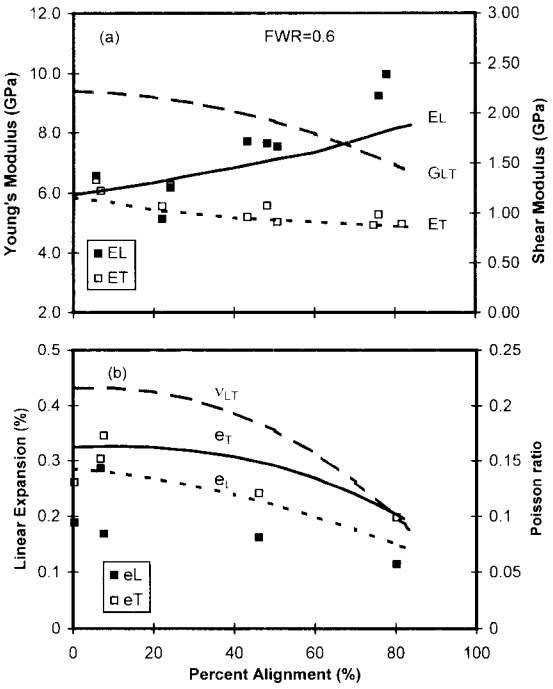

FIG. 8. Elastic constants and linear expansion of three-layer OSB as a function of percent alignment. (a) E_L, E_T, and G_{LT}; (b) e_L, e_T, and v_{LT}. Symbols show the experimental data of E_L, E_T, e_L, and e_T from board with specific gravity = 0.7 (Lee and Wu 2002).

The shear modulus for three-layer OSB decreased as PA increased at a given FWR (Fig. 8a). The trend is similar to that of single-layer OSB, and the value was slightly lower than that for the single-layer boards. Similar to shear modulus, Poisson ratio decreased as PA increased. The values are significantly smaller than those of single-layer boards due to cross lamination (i.e., reduced degree of orthotropy along a given direction). The decreasing trends in both shear modulus and Poisson ratio were

due to increased differential strength properties between face and core layers for three-layer boards at high alignment levels.

Typical LE data as a function of PA predicted by the model along the two principal directions are shown in Fig. 8b. Both e_L and e_T decreased as PA increased at FWR = 0.6. For a PA change from 0 to 80%, there were a 47% reduction in e_L and a 37% reduction in e_T, indicating a significant improvement in LE at higher alignment levels. At a given PA level, e_T had a higher value than e_L, showing the directional dependence of LE at the given FWR level. This trend varied with changes in FWR. The predicted LEs matched the measured data (Lee and Wu 2002) well, considering the large variability of the LE data. The trend of e_T for the three-layer boards differed significantly from that of single-layer OSB (Fig. 7b) due to the cross-lamination (i.e., restricting effects of the cross-laminated layer on wood transverse expansion). Xu (2000) predicted a similar trend of LE as a function of PA with his one-dimensional model.

Typical plots showing the influence of FWR at various PAs on effective modulus and linear expansion are shown in Fig. 9 (a: E_L and b: e_T). Also shown in Fig. 9 are the experimental data (symbols) from Lee and Wu (2002). Along a given direction, FWR significantly affected the magnitude of the modulus (Fig. 9a). With FWR < 0.5, increases in PA led to decreases of E_L, due to the dominating effect of the core layer. Above the FWR level, the face layer became dominated and E_L increased with increases in PA. There was little change of the modulus at FWR = 0.5 as PA increased. Thus, to enhance E_L by improving flake alignment level, FWR has to be controlled at levels greater than 0.5. The opposite is true for E_T. The predicted trends agreed well with experimental data at the selected FWR levels.

Typical plots showing combined effects of FWR and PA on LE are shown in Fig. 9b (e_T). FWR had no direct influence on LE for random boards. Increases of FWR caused e_T to increase (Fig. 9b) and e_L to decrease for the aligned boards. At a given FWR level, increases in PA led to decreases in e_T with FWR up to the 0.7 to 0.8 level. Above the FWR level, increases in PA led to increases of e_T. At FWR = 1.0, the board became single-layer and e_T increased significantly as PA increased. The opposite trend is generally true for e_L. The predicted LEs compared well with the experimental data at the selected FWR levels.

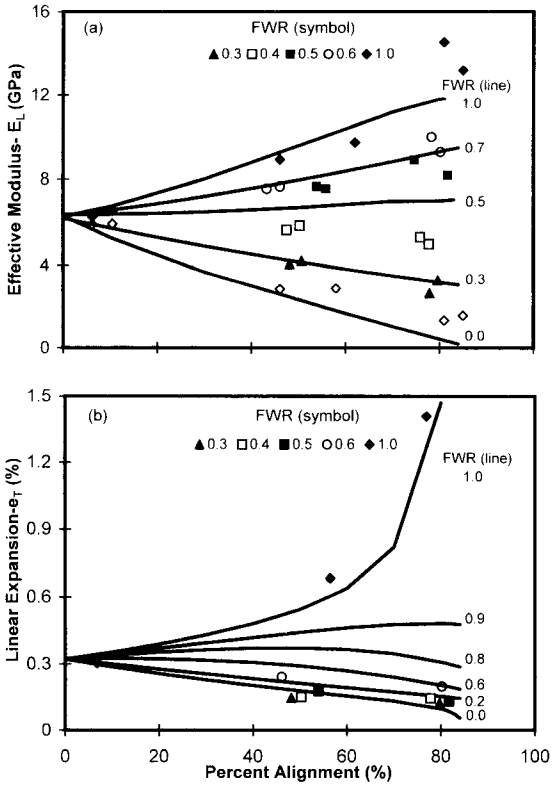

FIG. 9. Influence of FWR and PA on effective modulus and linear expansion. (a) E_L and (b) e_T. Symbols show the experimental data from boards with specific gravity = 0.7 (Lee and Wu 2002).

Simulation analysis

A simulation study was performed to predict engineering constants of OSB as a function of FWR and PA simultaneously using the model. The results of the analysis are shown as three-dimensional mesh plots in Figs. 10 and 11. The mesh in each graph is bordered with four sides representing:

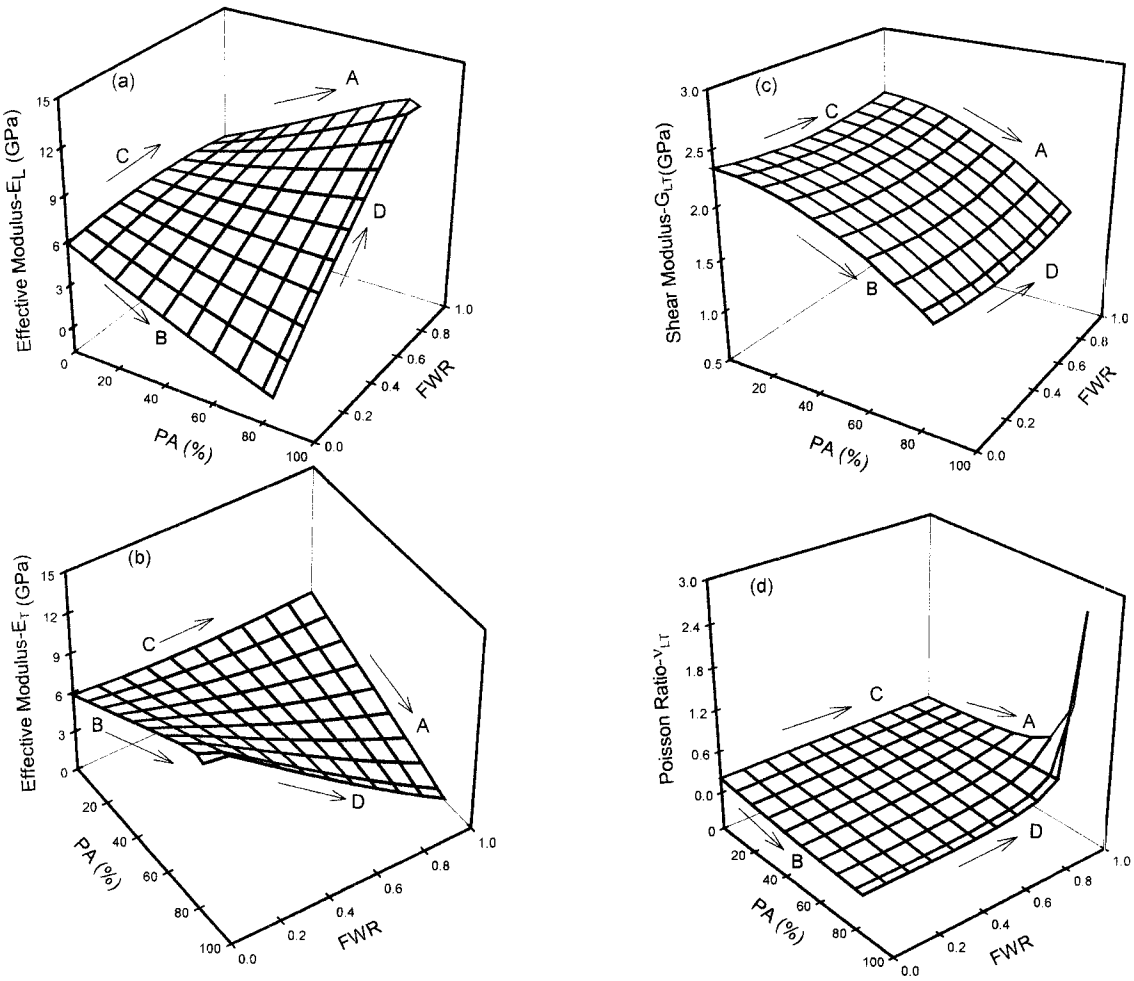

FIG. 10. Simulated elastic constants as a function of PA and FWR. (a): E_L, (b): E_T, (c): G_{LT}, and (d): ν_{LT}.

Side A: Single-layer boards (FWR = 1 face layer only) with varying PAs;
Side B: Single-layer boards (FWR = 0 core layer only) with varying PAs;
Side C: Three-layer boards (PA = 0%) with varying FWRs; and
Side D: Three-layer boards (PA = 85%) with varying FWRs.

The lines within the mesh represent three-layer boards of various structures. The following discussion is directed towards each individual property.

Effective modulus.—The predicted panel effective moduli, E_L and E_T, are shown in Figs. 10a and 10b, respectively. Along Side A, E_L increased and E_T decreased as PA increased. Along Side B, the opposite trend occurred. E_L decreased and E_T increased as PA increased. Along Side C, both E_L and E_T were a constant because these boards were with random flake orientation and FWR had no direct effects on the moduli. Along Side D, E_L increased and E_T decreased as FWR increased for the three-layer boards. E_L at FWR close to one and E_T at FWR close to zero leveled off somewhat. The transitional properties from Side A and Side B as influenced by FWR at each PA and from Side C to Side D as influenced by PA at each FWR are clearly shown in the graphs.

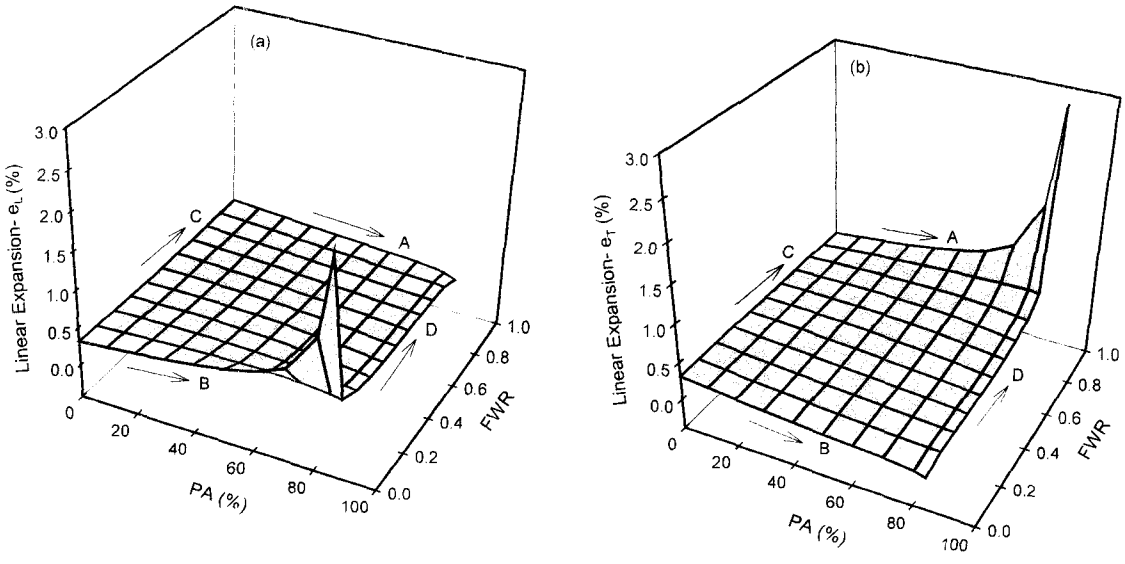

FIG. 11. Simulated linear expansion as a function of FWR and PA. (a) e_L and (b): e_T. Moisture content change = 9% from an initial value of 6%.

Shear modulus.—Predicted shear moduli at various FWRs and PAs are shown in Fig. 10c. Along Sides A and B, the modulus decreased in a curvilinear manner as PA increased, indicating a significant effect of flake alignment level on the shear modulus. Along Sides C and D, the modulus decreased as FWR increased, reached minimum at FWR = 0.5, and increased as FWR increased further. The surface was symmetric about the line at FWR = 0.5. The change of the modulus within the mesh as influenced by FWR and PA is clearly illustrated in the graph. The predicted trend of G_{LR} as influenced by FWR and PA was largely controlled by parameter a_2 of the PDF (Fig. 5b). Considering the importance of shear property in structural uses of OSB such as shear wall, the predicted trend of G_{LR} can be used to optimize the modulus by changing PA and/or FWR.

Poisson ratio.—Predicted Poisson ratios at various FWRs and PAs are shown in Fig. 10d. Along Side A, Poisson ratios increased as PA increased. The rate of change increased significantly with PA > 60%. Along Side B, there was a small decrease of ν_{LT} with PA increases. Along Side C, the values of ν_{LT} for boards with random alignment level were not influenced by FWR. Along Side D, FWR increases led to the increase of the Poisson ratio. The ratio increased rapidly when FWR was greater than 0.5. It reached the maximum at the corner defined by Sides A and D, indicating a very high degree of orthotropy in the range.

Linear expansion.—Predicted LEs at various FWRs and PAs are shown in Fig. 11a and 11b. Along Side A (single-layer boards with flake alignment levels varying from random to perfect alignment toward the MD), e_L decreased and e_T increased as PA increased. Along Side B (single-layer boards with flake alignment levels varying from random to perfect alignment toward the CD), the opposite trends occurred for e_L and e_T. Side C represents boards at random alignment levels, and the LE values for both e_L and e_T were a constant. Along Side D (three-layer boards with PA = 85%), e_L decreased and e_T increased as FWR increased. The value of e_L reached minimum and e_T reached maximum at the corner defined by Side A and Side D. At the corner defined by Sides B and D, e_L reached maximum, and e_T reached minimum. A similar

general trend of LE as influenced by PA and FWR was predicted by Xu (2000) in his one-dimensional model except that his model showed a significant influence of FWR on LE when PA = 0 (i.e., random boards along Side C), which is unexplainable.

SUMMARY AND CONCLUSIONS

The proposed laminate model based on the continuum theory is capable of predicting two-dimensional elastic moduli and linear expansion of OSB using parameters of experimentally determined flake properties and alignment distributions. Novelty of the model includes the construction of flake alignment PDFs for three-layer boards based on flake alignment distributions determined from the board surface, the combination of flake alignment PDFs with the classic lamination theory, and the use of two-dimensional flake and resin properties as model input.

The Halpin-Tsai equation predicted an enforcement effect of the flake moduli in the transverse direction due to resin application. Flake alignment distributions characterized by the two-term cosine PDF played its unique role in controlling the engineering constants of OSB. The continuum model predicted well-expected trends of the major engineering constants of OSB, including Young's and shear moduli, Poisson ratio, and linear expansion coefficients as influenced by PA and FWR. The predicted Young's moduli and LEs compared well with published experimental data of similar board structures. The predicted trends on individual properties allow examining interactions among the properties and process variables (i.e., PA and FWR) to optimize OSB's engineering performance.

The simulation model provides a basis of further model development that describes effects of flake length and void structure in OSB on its engineering constants.

ACKNOWLEDGMENTS

This study was supported by the USDA National Research Initiative Competitive Grant Program (99-35103-8298). The financial contribution to the project is gratefully acknowledged.

REFERENCES

AGARWAL, B. D., AND L. J. BROUTMAN. 1990. Analysis and performance of fiber composites, 2nd ed. Wiley Interscience Publ., New York, NY. 449 pp.

BARNES, D. 2000. Integrated model of the effect of processing parameters on the strength properties of oriented strand wood products. Forest Prod. J. 50(11/12):33–42.

BODIG, J., AND B. A. JAYNE. 1982. Mechanics of wood and wood composites. Van Nostrand Reinhold Company, New York, NY. 712 pp.

CHIN, W., H. T. LIU, AND Y. D. LEE. 1988. Effects of fiber length and orientation distribution on the elastic modulus of short fiber reinforced thermoplastics. Polymer Composites 9(1):27–35.

DAI, C., AND P. R. STEINER. 1994a. Spatial structure of wood composites in relation to processing and performance characteristics. Part 2. Modeling and simulation of a randomly-formed strand layer network. Wood Sci. Technol. 28(2):135–146.

———, AND ———. 1994. Spatial structure of wood composites in relation to processing and performance characteristics. Part 3. Modeling the formation of multilayered random strand mat. Wood Sci. Technol. 28(3): 229–239.

GEIMER, R. L. 1976. Flake alignment in particleboard as affected by machine variables and particle geometry. Research Paper FPL 275. USDA Forest Service, Forest Products Lab., Madison, WI.

———. 1979. Data basic to the engineering design of reconstituted flakeboard. Pages 105–125 *in* T. M. Maloney, ed. Proc. 13th WSU International Symposium on Particleboard. Washington State University, Pullman, WA.

———, R. J. MAHONEY, S. P. LOEHNERTZ, AND R. W. MEYER. 1985. Influence of processing-induced damage on strength of flakes and flakboards. Research Paper FPL 463. USDA Forest Service, Forest Products Lab., Madison, WI.

HALPIN, J. C., AND S. W. TSAI. 1969. Effects of environmental factors on composite materials. AFML-TR 67-423.

HARRIS, R. A., AND J. A. JOHNSON. 1982. Characterization of flake orientation in flakeboard by the von Mises probability distribution. Wood Fiber 14(4):254–266.

HUNT, M. O., AND S. K. SUDDARTH. 1974. Prediction of elastic constants of particleboard. Forest Prod. J. 24(5): 52–57.

JANOWIAK, J. J., D. P. HINDMAN, AND H. B. MANBECK. 2001. Orthotropic behavior of lumber composite materials. Wood Fiber Sci. 33(4):580–594.

JONES, R. M. 1975. Mechanics of composite materials. McGraw-Hill, New York, NY. 365 pp.

KELLY, M. W. 1977. Critical literature review of relationships between processing parameters and physical properties of particleboard. Gen. Tech. Rept. FPL-10. USDA Forest Serv., Forest Products Lab., Madison, WI. 65 pp.

LEE, J. N., AND Q. WU. 2002. In-plane dimensional stability of three-layer oriented strandboard. Wood Fiber Sci. 34(1):77–95.

LU, W., L. A. CARLSSON, AND Y. ANDERSSON. 1995. Micromodel of paper: part 1. Bounds on elastic properties. TAPPI J. 78(12):155–164.

PRICE, E. W. 1976. Determining tensile properties of sweetgum veneer flakes. Forest Prod. J. 26(10):50–53.

SALMEN, N. L., AND M. RIGDAHL. 1985. Modeling extensional stiffness for different paper structure. TAPPI. 68(2):105–109.

SCALA, E. 1973. Composite materials for combined functions. Haden Book Company, Inc., Rochelle Park, NJ.

SCHULGASSER, K. 1985. Fiber orientation in machine-made paper. J. Mater. Sci. 20:859–866.

———, AND D. H. PAGE. 1988. The influence of transverse fiber properties on the in-plane elastic behavior of paper. Composite Sci. Technol. 32:279–292.

SHALER, S. M., AND P. R. BLANKENHORN. 1990. Composite model prediction of elastic moduli for flakeboard. Wood Fiber Sci. 22(3):246–261.

STEINMETZ, P. E., AND C. W. POLLEY. 1974. Influence of fiber alignment of stiffness and dimensional stability of high-density dry-formed hardboard. Forest Prod. J. 24(5):45–50.

TSAI, S. W., AND H. T. HAHN. 1980. Introduction to composite materials. Technomic, CT.

USDA FOREST SERVICE. 1987. 1997. Wood handbook: Wood as an engineering material. Agric. Handb. No. 72. USDA Forest Prod. Lab., Madison, WI. 466 pp.

WU, Q. 1999. In-plane dimensional stability of oriented strand panel: Effect of processing variables. Wood Fiber Sci. 31(1):28–40.

———, AND O. SUCHSLAND. 1996. Linear expansion and its relationship to moisture content change for commercial oriented strand boards. Forest Prod. J. 46(11/12): 79–83.

XU, W. 2000. Influence of percent alignment and shelling ratio on linear expansion of oriented strandboard: A model investigation. Forest Prod. J. 50(7/8):88–93.

———, AND OTTO SUCHSLAND. 1997. Linear expansion of wood composites: A model. Wood Fiber Sci. 29(3): 272–281.